ELECTRON CLOUD OBSERVATIONS AND CURES IN RHIC*

W. Fischer[†], M. Blaskiewicz, M. Brennan, H. Huang, H.-C. Hseuh, V. Ptitsyn, T. Roser, P. Thieberger, D. Trbojevic, J. Wei, and S.Y. Zhang, BNL, Upton, NY 11973, USA
U. Iriso, CELLS, Bellaterra, Spain

Abstract

Since 2001 RHIC has experienced electron cloud effects, which have limited the beam intensity. These include dynamic pressure rises – including pressure instabilities, tune shifts, a reduction of the stability threshold for bunches crossing the transition energy, and possibly incoherent emittance growth. We summarize the main observations in operation and dedicated experiments, as well as countermeasures including baking, NEG coated warm beam pipes, solenoids, bunch patterns, anti-grazing rings, pre-pumped cold beam pipes, scrubbing, and operation with long bunches. This article is a short version of [1].

INTRODUCTION

The Relativistic Heavy Ion Collider (RHIC), in operation since 2000, has collided species from gold ions, at energies up to 100 GeV/n, to polarized protons, at energies up to 100 GeV [2]. Since 2001 dynamic pressure rises and other phenomena caused by electron clouds were observed. We summarize these observations, as well as countermeasures. Tab. 1 shows selected beam parameters.

OBSERVATIONS

Dynamic pressure rise. Large dynamic pressure rises were first observed in 2001 (Fig. 1) when the first attempt was made to double the number of bunches to 110. At that time the origin of the beam induced pressure rise was not known. As possible sources were considered: electron-impact desorption after an electron cloud has been formed, ion-impact desorption after rest gas ionization through the beam and subsequent acceleration of the ions in the beam potential, and desorption after beam loss.

Dynamic pressure rise from electron-impact desorption is also observed in other machines [5–8]. It was the first, and still is the most common electron cloud observation in RHIC [3, 14, 15]. It can be seen with all species (p, d, Cu, Au) at injection, transition (except protons that do not cross the transition energy), and store (Figs. 1 and 2).

In almost all operational situations the dynamic pressure rise is dominated by electron-impact desorption after an electron cloud was formed. There are, however, a few situations where this assumption cannot explain the observations. These are situations with large beam loss, the sudden pressure reduction in one of the experimental insertions, and pressure instabilities (see below).

The PHOBOS experiment (now decommissioned) had a uncoated Beryllium beam pipe. After rebucketing, when
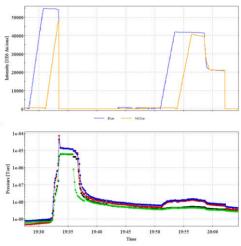

Figure 1: Beam intensities (top) and pressure in an interaction region (bottom). Shown are the first two attempts to fill both rings with 110 bunches, twice the design number (October 2001) [3].

the bunch length is shortened by half, an increase in the pressure by approximately one order of magnitude was observed (Fig. 2) [4]. The high pressure led to unacceptable experimental background, and was suddenly switched off after 30 min to 2 h. The sudden switch-off very likely requires that ions are involved in the pressure rise [17]. Without ions, the electron cloud density typically shows no second order phase transitions when the bunch intensity is changed by a small amount in simulations.

At transition the bunches are shortest, and the beams loose typically a few percent. However, the pressure rise occurs before beam loss is visible, and when sorted into bunch patterns the pressure rise is approximately proportional to the bunch intensity above a certain threshold. This feature is consistent with simulations [10].

In some instances pressure instabilities could be observed with gold beam, in an unbaked collimator location, and after an electron cloud was formed (Fig. 3). The formation of an electron cloud was triggered after rebucketing, when bunches are transferred from the accelerating rf system into the storage rf system. An analysis shows that such an instability is possible for gases like CO [13, 18, 19].

Tune shift. The coherent tune shift along a bunch train was measured at injection [16]. The sign of the

Table 1: Main beam parameters relevant to electron clouds.

parameter	unit	Au	Cu	d	p
revolution time T_{rev}	μs		12.8		
rigidity, inj./store	Tm		81/832		79/334
full bunch length, inj./store	ns		15/5		20/10
no. of bunches N	...		up to 111		
bunch spacing t_b	...		multiples of 108 ns		
ions per bunch N_b	10^9	1.1	50	110	200

05 Beam Dynamics and Electromagnetic Fields

D01 Beam Optics - Lattices, Correction Schemes, Transport

Table 2: Main parameters of the warm vacuum system.

parameter	unit	Au^{+79} p$^+$
pressure p_0	Torr	$1.0 \cdot 10^{-9}$
tube conductance c_{CO}	m^{4}s^{-1}	0.25
pumping speed S_{CO}	m^{3}s^{-1}	0.31
space betw. pumps $2L$	m	14

observed tune shift in both planes is consistent with the existence of electron clouds, and the value of the tune shift allowed a first estimate of the electron cloud density ($\rho_e = 10^{11} - 10^{12}$ m^{-3}). The lower estimates is for the assumption of electron clouds in the whole ring, the higher for the warm regions only.

The estimated densities made possible the first comparisons with simulations [16, 23], which use the model [24] for the secondary electron generation. Cloud densities of the same order of magnitude could be obtained in the simulations. The results are sensitive to a number of input parameters [16]. The coherent tune shift due to electron clouds has not created any operational problems.

Electrons. Shortly after the first electron cloud observations, up to 15 electron detectors were installed in the warm regions [25, 26]. The detector design is based on a PSR design [27], although similar detectors have been installed in other machines. With a multi-grid design it is possible to measure the cloud density, and the energy distribution of the electrons in the cloud.

For the electron-impact desorption, the cloud density averaged over one turn, the electron spectrum, and electron-impact desorption coefficient η_e are relevant. Fig. 4 shows this time-averaged electron detector signal together with a pressure reading, as Blue beam is injected. The pressure increase is proportional to the average electron loud density, which shows that the dynamic pressure rise is dominated by electron-impact desorption.

Fig. 5 exhibits 2 measured energy spectra, with a large fraction of low energy electrons, a peak around 10 eV, and extending to about 300 eV. The measured spectrum can be reproduced in simulations, also shown in Fig. 5 [28].

With measured cloud densities and pressures it is possible to extract electron-impact desorption coefficients η_e
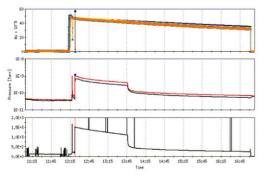

Figure 2: Pressure rise in PHOBOS after rebucketing. The intensity (top) slowly decays, and the pressure (middle) drops sharply after some time. With high pressure the experimental background (bottom) is increased [4].
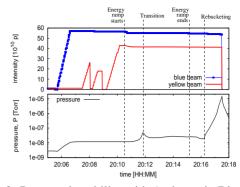
Figure 3: Pressure instability with Au beam in Blue. Total intensity for both rings during injection, acceleration, and storage (top), and pressure near the collimators (bottom), with an exponential increase after rebucketing [13].
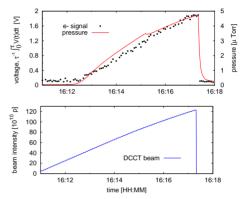

Figure 4: Pressure and electron signal evolution (top), as Blue beam is being injected (bottom) [28].

(Fig. 6). For an unbaked stainless steel beam pipe $\eta_e = 0.01 \pm 0.005$ molecules/electron (CO equivalent) is measured, after several months of conditioning in operation. The initial value is larger by approximately a factor 5. For a baked stainless steel pipe no conditioning is observable, and the measured electron-impact desorption coefficient is $\eta_e = 0.004 \pm 0.001$ [28].

Beam instabilities. In RHIC, the beam is most susceptible to instabilities at transition, which all species except protons cross. Transition crossing is facilitated with a γ_t-jump of fast ramping quadrupoles, since the main superconducting magnets ramp only slowly. Because the bunches are short, and the chromaticity across the transition energy is changed much slower than the γ_t-jump, bunches with enough intensity can become unstable. The observed instabilities are single bunch and transverse [29], with 2 typical growth times (15 ms and 120 ms). In addition to a careful chromaticity setting, octupoles are used to suppress instabilities. It was found that electron clouds, also enhanced by the short bunch length at transition, can reduce the stability threshold. This manifests itself through increasing beam losses along the bunch train, and was observed in dedicated experiments [30], as well as during operation in the recent Au run (Fig. 7). A review of single bunch instabilities driven by electron clouds is [31].

Emittance growth. Work on incoherent emittance growth from electron clouds is reported in [32,33], and may
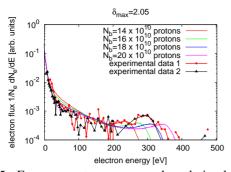
Figure 5: Energy spectrum measured, and simulated for $\delta_{\max} = 2.05$ and different bunch intensities. The spectrum shape is not significantly affected by δ_{max} [28].
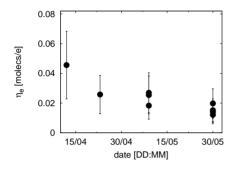

Figure 6: Calculated desorption coefficients for an unbaked stainless steel surface. A decrease of the desorption coefficient with time is noticeable due to scrubbing [28].

also be relevant to the RHIC polarized proton operation. In the most recent polarized proton run, bunches shortened through rf quadrupole pumping in the AGS were injected in order to increase the luminosity through the reduction of the hour-glass effect at store. However, the luminosity of the stores with bunches of reduced length was lower than the luminosity of stores with longer bunches of comparable intensity (Fig. 8) [34]. At the same time, a higher dynamic pressure was observed at injection. This could be an indication that electron clouds at injection have increased the proton beam emittance.

CURES

In-situ baking. The warm beam pipes are made of stainless steel 304L. Due to scheduling constraints, most warm beam pipes were not baked in-situ initially. After the first dynamic pressure rises were observed, a program was started to bake in-situ all warm pipes, yielded the first sig-
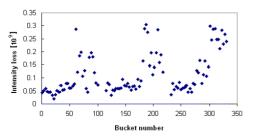

Figure 7: Yellow beam loss at transition along the bunch train. 8 bunches are missing after 1/3 and 2/3 of the length. The losses increase until a gap is reached, then fall.
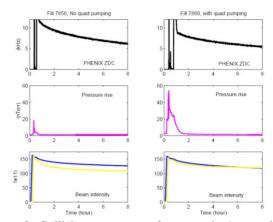
Figure 8: Collision rates, sum of pressure in 4 warm locations, and intensity for two stores. The left column shows the standard situation, the right column a store for which shorter bunches were injected [34].

nificant increase in the beam intensity. With the exception of a few instruments, and the warm rf, baking is possible at all other locations.

NEG coating. Thin-film coating of beam pipes with the non-evaporable getter material TiZrV has been developed at CERN [35, 36], and found large-scale applications in a number of machines [9, 37–40]. Properties of NEG coated surfaces are reported in [40–42]. 55 m of NEG coated beam pipes were installed in 2003, for tests in 2004, and for comparisons with solenoids. After evaluation, a decision was made to replace as much of the approximately 700 m of warm beam pipes as possible with NEG coated ones. This is possible for 520 m, and until 2007 475 m were replaced. The NEG coating was done by SAES Getter. Fig. 9 shows that the dynamic pressure in the 12 Blue warm sections in 2004, 2005, and 2006 decreases by orders of magnitude even with increasing beam intensity.
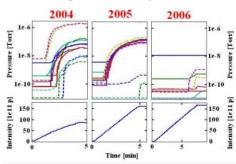

Figure 9: Dynamic pressure in 12 Blue warm straight sections (top) while proton beam with 108 ns bunch spacing is filled (bottom), in 2004-2006 [39].

Solenoids. In 2003 60 m of solenoids were installed in the warm sections to evaluate their effect on the dynamic pressure rise. Solenoids had been successfully used in other machines [6, 43, 44]. Fig. 10 shows a test of the solenoid effectiveness in suppressing the dynamic pressure rise. At a magnetic field of 1.35 mT a reduction of both the electron cloud density, and the pressure is observable. The suppression is not stronger when the field is increased
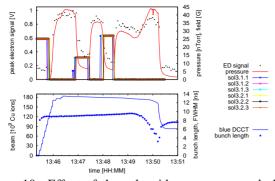
Figure 10: Effect of the solenoid on pressure and electron detector signal. Both decrease for a magnetic field of 1.35 mT and 2.7 mT. At 13:49:30 acceleration starts, the bunch length is reduced, and pressure and electron signals increase. Half of the beam is lost at transition [25].

to 2.7 mT. In other tests the field has been increased up to 6 mT, but generally the dynamic pressure increase could not be suppressed completely.

Bunch patterns. Below the beam-beam limit the same total intensity gives a higher luminosity when concentrated in fewer bunches. Simulations and beam tests showed that this also minimizes the electron cloud density when the bunches are uniformly distributed around the circumference [45]. This is shown in Fig. 11 for 68 bunches. Between the top and bottom case, the peak electron cloud density is reduced by about a factor 5, the average density even more. The optimization of bunch pattern lends itself to analysis through maps [46].

In the 2004 Au-Au run the beam intensity was limited by pressure rises in PHOBOS (Fig. 2). During the run the number of bunches was reduced from 61 to 56 to 45 (all approximately uniformly distributed) as more bunch intensity became available from the injectors, thus increasing the luminsity at the electron cloud limit. With the same limit in place for the 2005 Cu-Cu run, the number of bunches could be even further reduced to 37.

Anti-grazing rings. Lost beam particles hitting the beam pipe under a grazing incident angle penetrate the beam pipe surface many times due to the surface roughness (Fig. 12). This is expected to lead to electron and molecular desorption coefficients about two orders of magnitude higher than for perpendicular impact. In [47] a mitigation was proposed by installing anti-grazing rings, through which all particles are lost with near perpendicular impact. For a test 5 anti-grazing rings each were installed in 2 sections in RHIC, and a reduction in the dynamic pressure rise could be observed [48]. However, for the rings to be effective, they must intercept beam, which could lead to increased experimental background if they are close to a detector and beam is intercepted there which would be lost elsewhere otherwise. With the large-scale installation of NEG coated beam pipes, currently no anti-grazing rings are installed in RHIC.

Pre-pumping in cold sections. At high proton beam intensities an increase in the gas density in the cold sec-
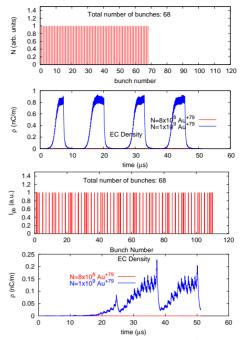

Figure 11: Simulated electron cloud evolution over 4 turns for 68 Au bunches with a single gap of maximum lengths (top), and with approximately uniform distribution [45].
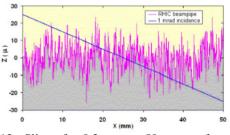

Figure 12: Slice of a 0.2 mm × 50 mm surface scan of RHIC beam pipe material obtained by Solarius, Inc. An ion trajectory incident at 1 mrad is superimposed [47].

tions was observed. The cold sections initially relied on cryo-pumping, and had been evacuated before cool-down, to about 10^{-1} Torr only in some areas, leading to approximately 5 mono-layers. Near a warm-cold transition there can be many more mono-layers. Small ion pumps were installed permanently in these regions, which evacuated the beam pipe to 10^{-6} to 10^{-7} Torr before cool-down. No further increases in the gas density were observed.

Scrubbing. Scrubbing is used routinely in the SPS [5], and had been tested in RHIC in 2004 [49]. After a few hours of scrubbing a reduction of the pressure rise by some 10% was observed in locations with the highest pressure.

At the beginning of the 2007 gold-gold run pressures up to 10^{-6} Torr were observed near the warm rf and a few other locations that can not be baked at high temperature. Two hours of scrubbing at injection with the highest available ion intensities, reduced the dynamic pressure by approximately one order of magnitude at the locations with the highest pressure (Fig. 13).

Operation with longer bunches. The electron cloud is enhanced with shortened bunches (Fig. 3). At transition,

05 Beam Dynamics and Electromagnetic Fields

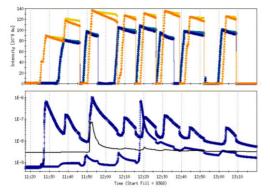D01 Beam Optics - Lattices, Correction Schemes, Transport

Figure 13: Scrubbing during the 2007 Au operation.

the rf voltage has been reduced from 300 kV to 150 kV to lengthen the bunches, and reduce the electron cloud density. Experiments had shown that this reduces the intensity loss along the bunch train [30]. To avoid the possible incoherent emittance growth at injection with protons, and also allow for better longitdinal injection matching, a new rf system with harmonic number 120 is under construction (the current system has $h = 360$) [50].

SUMMARY

Since 2001 electron cloud effects have limited the beam intensity in RHIC. The most common effect is dynamic pressure rise, which occurred with all species, and at injection, transition, and store. Other pressure rise mechanism were investigated but are not important in normal operation. In some cases, pressure instabilities were observed.

The beam intensity can also be limited because electron clouds lower the stability threshold of bunches crossing the transition energy. Recently, incoherent transverse emittance growth has been observed with protons at injection, possibly caused by electron cloud.

The main cure for electron clouds in the warm sections are NEG coated beam pipes. In the cold regions, additional pumps reduced the pressure before cool-down, leading to less than a mono-layer of molecules after cool-down. Other cures tested or used, include solenoids, optimized bunch patterns, anti-grazing rings, scrubbing, and long bunches.

ACKNOWLEDGMENTS

REFERENCES

[1] W. Fischer et al., ELOUD'07, Daegu, Korea (2007).

[2] W. Fischer, EPAC'06, Edingburgh, UK (2006).

[3] W. Fischer et al., EPAC'02, Paris, France (2002).

[4] G. Rumolo and W. Fischer, BNL C-A/AP/146 (2004).

[5] G. Arduini et al., ECLOUD'04, Napa, CA (2004).

[6] A. Kulikov, A. Novokhatski, and J. Seeman, ECLOUD'04, Napa, CA (2007).

[7] R.J. Macek et al., ECLOUD'04, Napa, CA (2004).

[8] R. Zwaska, ECLOUD'07, Daegu, Korea (2007).

[9] J. Pasternak et al., PAC'05, Knoxville (2005).

[10] W. Fischer and U. Iriso, BNL C-A/AP/184 (2004).

[11] Y.-K. Kim et al., NIST physics reference data for electron-impact cross sections for ionization and excitation, http://physics.nist.gov/PhysRefData/Ionization/ (2004).

[12] F.F. Rieke, W. Prepejchal, Phys. Rev. A **4**, p. 1507 (1972).

[13] W. Fischer, U. Iriso, and E. Mustafin, AIP Conf. Proc. **773**, pp. 204-206 (2004).

[14] U. Iriso et al., EPAC'04, Lucern, Switzerland (2004).

[15] S.Y. Zhang et al., PAC'05, Knoxville, TN (2005).

[16] W. Fischer et al., Phys. Rev. ST Accel. Beams 5, 124401 (2002).

[17] U. Iriso and S. Peggs, Phys. Rev. ST - Accel. Beams **9**, 071002 (2006).

[18] E. Mustafin et al., AIP Conf. Proc. **773**, p. 222-225 (2004).

[19] S.Y. Zhang, BNL C-A/AP/190 (2005).

[20] M.A. Furman, A.A. Zholents, PAC'99, New York (1999).

[21] F. Zimmermann, PAC'01 (2001).

[22] K. Ohmi, S. Heifets, and F. Zimmermann, APAC'01, Beijing; CERN SL-2001-062 (AP) (2001).

[23] M. Blaskiewicz and U. Iriso, BNL C-A/AP/260 (2006).

[24] M.A. Furman and M. Pivi, Phys. Rev. ST - Accel. Beams **5**, 124404 (2002).

[25] U. Iriso, Ph.D. thesis, University of Barcelona, BNL C-A/AP/228 (2006).

[26] U. Iriso et al., PAC'03, Portland, OR (2003).

[27] R. Macek et al., Workshop on Two Stream Instabilities, KEK, Tsukuba, Japan (2001).

[28] U. Iriso and W. Fischer, Phys. Rev. ST - Accel. Beams **8**, 113201 (2005).

[29] M. Blaskiewicz et al., PAC'03, Portland, OR (2003).

[30] J. Wei et al., HB2006, Tsukuba, Japan (2006).

[31] F. Zimmermann, Phys. Rev. ST - Accel. Beams **7**, 124801 (2004).

[32] E. Benedetto, G. Franchetti, and F. Zimmermann, PRL **97**, 034801 (2006).

[33] K. Ohmi and K. Oide, Phys. Rev. ST - Accel. Beams **10**, 014401 (2007).

[34] S.Y. Zhang, V. Ptitsyn, ECLOUD'07, Daegu, Korea (2007)

[35] C. Benvenuti et al., Vacuum **60**, pp. 57-65 (2001).

[36] C. Benvenuti et al., J. Vac. Sci. Technol. A **16** (1998).

[37] M. Hahn, R. Kersevan, I. Parat, EPAC'06 (2006).

[38] S.Y. Zhang et al., BNL C-A/AP/220 (2005).

[39] S.Y. Zhang et al., EPAC'06 (2006).

[40] P. Chiggiato and P. Costa Pinto, Thin Film Solids **515**, pp. 382-388 (2006).

[41] C. Scheuerlein et al., Applied Surface Science **172**, pp. 95-102 (2001).

[42] M. Nishiwaki, S. Kato, ELOUD'07, Daegu, Korea (2007).

[43] H. Fukuma, ECLOUD'07, Napa, CA (2007).

[44] J.Q. Wang et al., ECLOUD'04, Napa, CA (2007).

[45] W. Fischer and U. Iriso, EPAC'04 (2004).

[46] U. Iriso and S. Peggs, Phys. Rev. ST - Accel. Beams **8**, 024403 (2005).

[47] P. Thieberger et al., Phys. Rev. ST - Accel. Beams **7**, 093201 (2004).

[48] S.Y. Zhang et al., Phys. Rev. ST - Accel. Beams **8**, 123201 (2005).

[49] S.Y. Zhang, et al., EPAC'04 (2004).

[50] M. Brennan and A. Zaltsman, private communication (2007).

05 Beam Dynamics and Electromagnetic Fields

D01 Beam Optics - Lattices, Correction Schemes, Transport